NANO LETTERS

2004
Vol. 4, No. 12
2403−2407

Thermal Interface Properties of Cu-filled Vertically Aligned Carbon Nanofiber Arrays

Quoc Ngo,[†,‡] Brett A. Cruden,[‡] Alan M. Cassell,[‡] Gerard Sims,[‡] M. Meyyappan,[‡] Jun Li,[*,‡] and Cary Y. Yang[†]

Center for Nanostructures, Santa Clara University, Santa Clara, California 95050, and Center for Nanotechnology, NASA Ames Research Center, Moffett Field, California 94035

Received September 13, 2004; Revised Manuscript Received October 24, 2004

ABSTRACT

Nanoengineered materials have emerged as efficient thermal interface materials in a variety of thermal management applications. For example, integrated circuits (IC) are subject to tight thermal budgets to maintain acceptable reliability standards. This letter presents thermal contact resistance measurement results and analyses for copper gap-filled carbon nanofiber–copper composite arrays. Experimental results demonstrate the efficient interfacial thermal conduction of these structures. Using copper as a gap-fill material for improving lateral heat spreading and mechanical stability is discussed.

Thermal characteristics of multiwall carbon nanotubes (MWNTs) have been measured,[1−4] revealing their unique thermal conductivity characteristics along the nanotube axis. For a discrete MWNT, thermal conductivity has been measured surpassing 3000 W m^{-1} K^{-1} in the axial direction.[1] Other studies have reported values for discrete MWNTs as small as 15 (W m^{-1} K^{-1})[2] and 27 (W m^{-1} K^{-1}).[3] The wide variation can be attributed to the inherently disordered nature of some carbon nanostructures grown by the chemical vapor deposition (CVD) process.[5] Concerns about the degradation of thermal conductivity in vertically aligned carbon nanofiber (VACNF) arrays due to poorly graphitized structures are valid when considering these structures in thin film applications where the intrinsic film properties are of great importance. In cases of studying thermal contact resistance, however, the physical nature of the contact between the nanofiber ends and hot contact surface tends to take precedence. It has been shown that as-grown carbon nanotube and nanofiber arrays have the potential to significantly improve thermal contact conductance.[6,7] However, to convert this into a manufacturable solution, care needs to be taken so that the array can withstand the rigorous mechanical stress in packaging process flows. Gap-filling copper between VACNFs provides a suitable mechanical anchor for the nanofibers to the substrate while also serving as a lateral heat spreader. The robust physical characteristics of the CNF−Cu composite also allow us to take advantage of increased contact surface area to the target material.

Progress in the scaling of integrated circuits has resulted in an alarming rise in power dissipation in high-density, high-frequency, silicon-based microprocessors.[8] The need for addressing this problem is imperative for maintaining reliability standards for next-generation IC packaging technology.[9,10] The knowledge gained from addressing issues in microprocessor packaging can also be generalized to most devices that exhibit high power dissipation. The space program at NASA is also in need of thermal interface materials to draw heat away from hot spots on critical electronic components. One of the current issues with cooling systems for space vessels is the degradation of such systems over time. Liquid-cooled systems and those with moving parts do not fit this requirement due to their lack of stability and the need for constant servicing. Carbon nanofiber composites are a strong candidate material to provide thermal solutions for space missions.

Through the use of DC-powered PECVD,[5] we fabricate vertically aligned, free-standing CNF arrays on silicon wafers of ~500 μm thickness. Copper electrodeposition, a common process used for gap-filling high aspect ratio trenches, is used for the creation of a CNF−Cu composite array. The data presented here demonstrate the mechanical strength and efficient interfacial heat conduction of CNF−Cu composite arrays suitable for next-generation heat-sink devices.

CNF arrays were grown using the procedure and reactor conditions detailed in ref 5. A layer of titanium (300 Å) was used as both an adhesion layer for a thin layer of nickel

* Corresponding author. E-mail: jli@mail.arc.nasa.gov; phone (650) 604-6459; fax (650) 604-5244.
[†] Santa Clara University.
[‡] NASA Ames Research Center.

10.1021/nl048506t CCC: $27.50 © 2004 American Chemical Society
Published on Web 11/13/2004

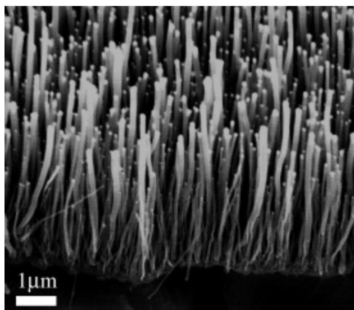

Figure 1. SEM micrograph of as-grown CNF array taken at 45° viewing angle.

catalyst used for the CNF array growth and as a seed layer for the subsequent copper electrodeposition. The resulting as-grown VACNFs are shown in Figure 1. From these images, we estimate the length of the nanofibers as approximately 7.5 μm. This information allows us to determine a target for how much copper should be deposited. The nanofiber lengths can be controlled from 1 to 30 μm by tuning the PECVD conditions. The CNF array has a random lateral distribution with an approximate average spacing of 200 nm to 300 nm. The interstitial space presents ~25:1 to 100:1 aspect ratio, necessitating super-filling of copper in these gaps.

Due to stringent processing and technology requirements for copper interconnect structures in ICs,[9] many processes have had the need to fabricate high aspect ratio copper interconnect structures. One such approach is the use of copper electrodeposition with a combination of additives in the electrolyte bath to promote "bottom-up" growth of narrow copper features.[11] The deposition in this work is performed in a three electrode setup with the VACNF sample (with a typical size of 1−2 cm^2) as the working electrode (WE), a saturated calomel electrode (SCE) as the reference electrode, and a one square inch platinum foil as the counter electrode (CE), set in parallel with the VACNF sample. The bath composition is 100 ppm chloride ions (Cl^-), 400 ppm polyethylene glycol (PEG) with a molecular weight of 8000, 10 ppm bis(2-sulfopropyl) disulfide (SPS), 10 ppm Janus Green B (JGB), 0.6 mol/L copper sulfate ($CuSO_4 \cdot 5H_2O$), and 1.85 mol/L sulfuric acid (H_2SO_4). In the presence of Cl^-, PEG molecules adsorb on the top of the high aspect ratio nanostructure and inhibit the Cu electrodeposition from sealing off the gap. SPS and JGB are used to accelerate the electrodeposition rate within the trench,[11] thereby achieving "bottom-up" gap filling from the Ti seed layer (WE). The deposition quality is a function of a variety of parameters such as electropotential, time, the selection of seed layer metal, as well as length distribution and density of the nanofiber array. Figure 2 shows the effect of different additive concentrations, resulting in different copper grain sizes. The potential (current) and time determine copper deposition rate and amount of copper deposited, respectively. Trials varying potential were conducted to find the optimal gap-filling conditions, which were determined to be −0.2 V (vs SCE) at a deposition rate of ~430 nm/min. By integrating the current with respect to time, we can determine the amount of charge that was deposited on the sample, thus determining the approximate amount of copper deposited. Using this method and correlating with SEM images, we estimate the copper to contain 20−30% submicron voids. The underlying metal seed layer, acting as the WE, must be a suitable electrode material such that it exhibits good electrochemical interaction with the electrolyte solution. When investigating chromium as the WE material, we found adequate filling characteristics in the interstitial spaces between nanofibers,[12] however, leaving significant amounts of voids at the Cr surface. Vastly improved bottom-up fill was achieved by using titanium as the WE. Figure 3 shows a comparison of the gap-filling characteristics by using the two different types of electrode material. Based on these data for titanium, we expect an enhancement in the lateral heat-spreading capabilities of the structure, as well as a more mechanically robust structure owing to decreased porosity of the copper material compared to using chromium as the seed layer.

While the resulting electrodeposition process (Figure 3) can be reliably controlled by altering deposition time, it provides a very rough copper surface and, in some cases, leaves copper at the ends of the nanofibers. Therefore, an etch step has been introduced to smooth the copper surface[13] as well as etch the extraneous copper from the nanofiber ends. This is done in an 85% ortho-phosphoric acid solution using the same three-electrode setup as in the deposition process at a potential of 1.5 V (vs SCE). A short, 45 s etch was used, resulting in the structure seen in Figure 4. When comparing Figure 5a to Figure 5b, one can see the absence of the nickel catalyst particle at the tip of the CNF, which is

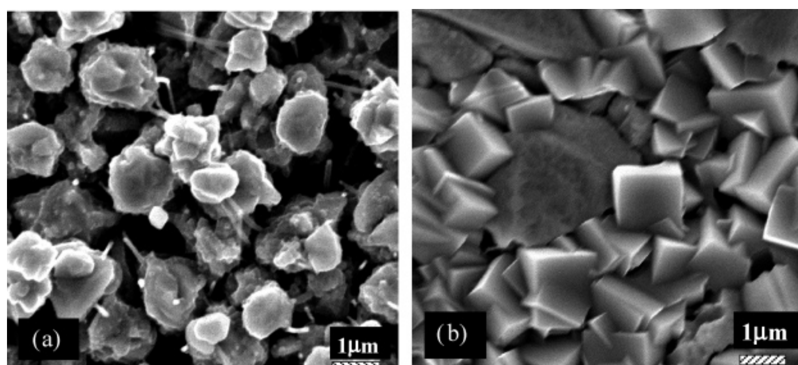

Figure 2. Top-down SEM micrographs of CNF−Cu composite (a) with optimized recipe and (b) initial recipe with no additives.

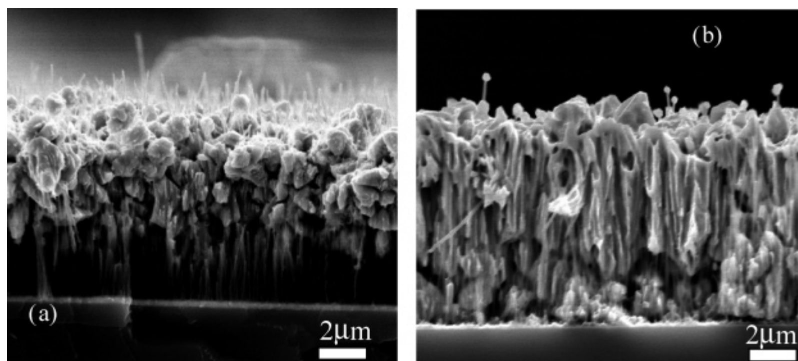

Figure 3. Comparison of copper gap-fill using (a) chromium and (b) titanium as the working electrode.

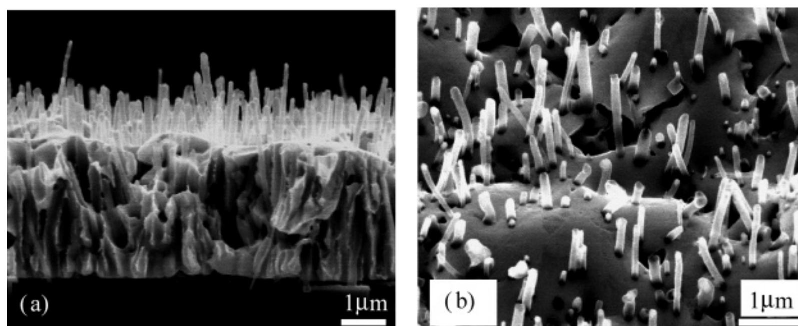

Figure 4. (a) Cross-sectional and (b) 45° angle view of CNF−Cu composite after 45 s copper etch in 85% orthophosphoric acid solution.

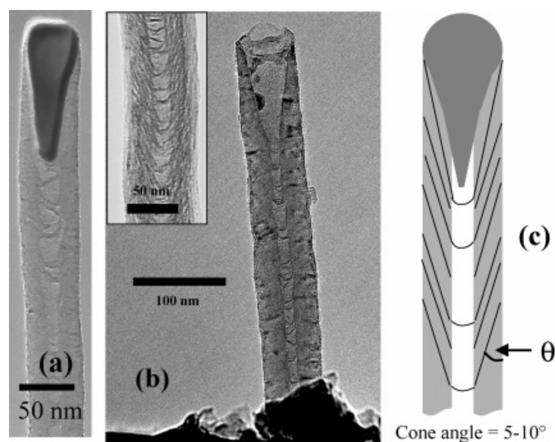

Figure 5. (a) TEM image of as-grown CNF tip. (b) CNF tip embedded in copper matrix after copper etch. Note that the nickel catalyst particle has been etched away from the tip. Inset: high magnification TEM showing CNF wall structure. (c) Schematic of CNF tip depicting typical cone angles.

removed in the highly acidic copper etch solution. We also observe from the images in Figures 5a and 5b that there are graphene crossover points along the length of the CNF. This disordered graphitic structure is inherent in VACNFs grown using the PECVD method.[5,14] Figure 5c shows a schematic of the nanofiber structures, exhibiting approximately a 5−10° cone angle deduced from high-resolution TEM of the sidewall of the CNFs. It is as yet uncertain how much this disordered structure affects the heat transport through the fiber in the axial direction. However, we postulate that the vertical alignment aids in lowering thermal contact resistance by ensuring most nanofibers will be contacted at the tip rather than the sidewall.

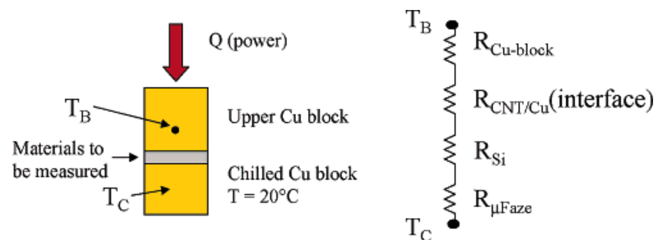

Figure 6. Apparatus used for thermal resistance measurement and equivalent thermal resistance model. T_B is the temperature of the block, measured using an embedded thermocouple.

An apparatus consisting of two copper blocks, four resistive cartridge heaters (not shown) embedded in the upper block, and a cooling bath was used to measure the thermal resistance of a given material[7] (Figure 6). The upper copper block is surrounded by insulation to minimize heat loss to the ambient, with the exception of the one square inch section designed to contact the material to be measured. The clamping pressure on the sample is controlled by pneumatically manipulating the upper block. Heat is delivered to the system by applying a constant power to the resistive heaters. Heat flux across the block is measured using the steady-state temperature difference ($\Delta T = T_B - T_C$) between the two blocks (and consequently, the sample). From these data, the thermal resistance of the sample is calculated as shown in eq 1,

$$R = \frac{A(T_B - T_C)}{Q - C_L(T_B - T_{amb})} \quad (1)$$

where Q is the total power, A is the sample area, and T_B, T_C, and T_{amb} represent the temperature of the upper block, the

chilled lower block (20 °C), and the ambient environment, respectively. C_L is a heat transfer coefficient used to estimate the heat loss to the ambient in this measurement configuration and is determined by placing a thick insulator between the two blocks and measuring the steady state ΔT at a variety of constant powers, yielding $C_L = 0.0939$ W/K.

The dominant thermal resistance in this measurement configuration is that of the contact interfaces between the sample and the copper blocks. To minimize this contact resistance on the rough side of the sample, two steps were taken: (1) polishing both copper block interfaces to reduce the effect of surface roughness, and (2) making use of a high thermally conductive, conformal material, Microfaze A6 (AOS Thermal Compounds, LLC) to reduce contact resistance on the backside of a silicon wafer, the substrate on which the investigated films were fabricated. Microfaze A6 consists of two gel-like materials of ~50 μm sandwiching an aluminum film (~50 μm) and is currently used as a compliant thermal interface material in many applications. Using the thermally conductive material on the rough side (backside of Si) allows us to characterize the CNF−Cu composite interface more reliably, as the Microfaze A6 should reduce the thermal contact resistance such that it is comparable or less than the resistance of the CNF−Cu composite material.

As can be seen in the equivalent resistance model (Figure 6), the measurement discussed previously encompasses all resistance components of the structure, including the upper copper block resistance, the CNF−Cu composite interface resistance, the intrinsic silicon resistance, and the Microfaze A6 resistance. The particular interface we are interested in is the upper block to CNF−Cu composite interface. The characterization of this film alone is accomplished through determination of the copper block thermal resistance and two control measurements involving the bare silicon interface and Microfaze A6. $R_{\mathrm{Cu-block}}$ is calculated assuming a linear variation of thermal resistance inside the block, from the thermocouple embedded 1.3 in. from the surface to the actual block interface. Using this assumption, we determine this value to be 0.83 cm^2 K/W for a one square-inch area based on bulk copper properties. For smaller sample sizes, the area is normalized to calculate the Cu-block resistance value. The control measurements are used to account for the resistance of the silicon, copper block, and Microfaze A6, allowing us to de-embed these contributions to determine resistance values of the CNF−Cu composite. To summarize, we can determine the interfacial contact resistance of the CNF−Cu composite interface when contacting the copper block by eq 2.

$$R_{\mathrm{CNT-Cu}}(\mathrm{interface}) = R_{\mathrm{total}} - R_{\mathrm{Cu-block}} - R_{\mathrm{Si}} - R_{\mu\mathrm{Faze}} \quad (2)$$

where R_{Si} is the intrinsic resistance of the silicon. For the 500 μm thick silicon wafer considered here, the calculated value of thermal resistance is 0.034 cm^2 K/W, which is approximately 2 orders of magnitude below the final measured values of the CNF−Cu sample and thus can be neglected in this case. Two control measurements are used

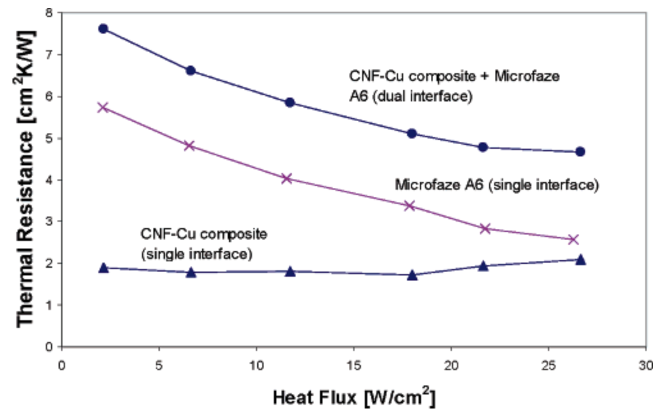

Figure 7. Thermal resistance versus power for CNF−Cu composite film at 6.8 psi clamping pressure. The upper curves show the measurement result before de-embedding the silicon and Microfaze A6. After correction, the thermal resistance values are fairly constant at different heat flux.

to determine $R_{\mu\mathrm{Faze}}$. The first measurement involves measuring the thermal resistance of a bare piece of silicon with Microfaze A6 on the backside of the wafer. This number gives $R_{\mathrm{control,1}} = R_{\mathrm{Cu-block}} + R_{\mathrm{block-Si}} + R_{\mu\mathrm{Faze}} + R_{\mathrm{Si}}$ where $R_{\mathrm{block-Si}}$ is the interfacial resistance between the copper block and silicon wafer. The second control measurement involves characterizing a double-sided polished piece of silicon wafer, giving us $R_{\mathrm{control,2}} = 2R_{\mathrm{block-Si}} + R_{\mathrm{Si}} + R_{\mathrm{Cu-block}}$. Thus far, the description of the measurement has not taken into account the changing properties of the Microfaze A6. The manufacturer's data suggest resistances as low as 0.13 cm^2 K/W at the ASTM D-5470 standard.[15] This number will not be attainable in our measurements due to two important factors: pressure and temperature. This ASTM standard is performed at a fixed pressure of 435 psi and a fixed average temperature 50 °C. Our measurements are performed at pressures much lower than these (from 7 to 70 psi) and at a variety of different temperatures, modulated by varying power input (Q) to the system. By using the two-step control measurement, we can effectively account for the power and pressure variation of the material under test.

Figure 7 shows thermal resistance measured with respect to heat flux for a CNF−Cu composite film before and after correcting for the power dependence of the Microfaze A6. Constant thermal resistance values obtained for the nanofiber composite film at different heat fluxes demonstrate the validity of the control sample correction scheme. The Microfaze A6, however, shows a decrease in thermal resistance with increasing heat flux. This can be explained by the polymeric composition of the material. The material mobility in the Microfaze A6 works to minimize thermal contact resistance under increasing heat flux by microscopically changing to fill voids in the thin polymer layer. In addition, the thixotropic nature of this interface material allows it to maintain its gel-like properties even under high heat flux conditions. The CNF−Cu composite material clearly eliminates any change in mobility caused by heat flux variation. Figure 8 shows thermal resistance measured for The Microfaze A6 interface, a single silicon interface, and the CNF−Cu composite film interface at different pressures.

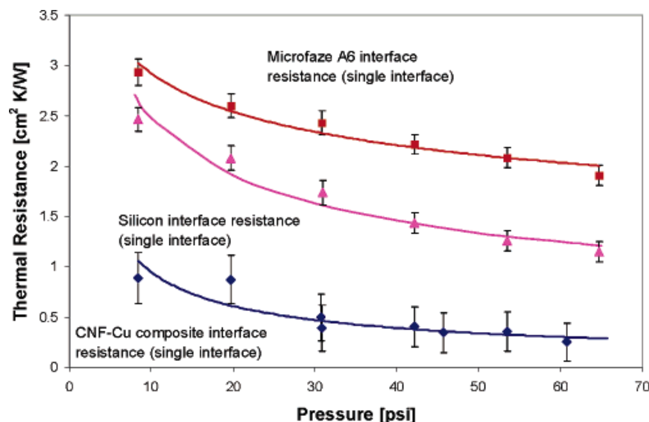

Figure 8. Thermal contact resistance versus pressure for CNF−Cu composite film at input power of 27.2 W. The two upper curves show the measurement result considering the Microfaze A6 and single silicon interface with the copper block, respectively. The lower curve represents the interfacial resistance of the composite film with the copper block. The solid lines represent the best fit data trends.

In this case, the resistance decreased with increasing pressure, which is consistent behavior for most thermal interface materials. It also shows that the VACNFs provide a better contact at increased pressure.

A good point of comparison for the CNF−Cu composite film would be an as-grown CNF array exhibiting roughly the same length and diameter distribution. Such a structure can demonstrate the usefulness of copper gap-filling in the array structure. Indeed, as shown in ref 12, the CNF array shows an increase in thermal resistance when compared to the CNF−Cu composite. The mechanism for such a difference in contact resistance can be explained by examining the structure of the CNFs. The disordered nature of the nanofibers exhibiting graphitic layers crossing the nanofiber axis[5,14,17] has been shown to demonstrate good electrochemical properties on active sites located on nanofiber sidewalls.[16] These active sites on the nanofibers allow heat to be conducted laterally in the composite array, dissipating the heat through the surrounding copper matrix as well as the VACNFs.

While the thermal resistance data presented here show promising trends for implementing CNF−Cu composite films as thermal interface materials in microelectronics packaging, this measurement technique can be optimized to minimize uncertainty in the thermal resistance values obtained. Improving surface roughness and temperature monitoring of the copper blocks are two such activities that need to be undertaken for more reliable thermal contact characterization. The composite film also holds the potential for further optimization by systematically studying the effect of Cu gap-fill on the structure's lateral heat spreading capability. This can be done by considering the effects of each additive to the electrolyte bath for copper deposition. Finally, a study of the mechanical deformation of the CNF ends should be performed to evaluate the mechanical properties of the interface between the CNF−Cu composite and heated copper surface.

In this letter we have demonstrated the efficient thermal contact conductance properties of CNF−Cu composite materials. The composite material considered here has been tested at a variety of powers and pressures, yielding reasonable trends indicating the viability of their use as a thermal interface material in both IC packaging and equipment cooling applications. Values of thermal resistance as low as 0.25 cm^2 K/W have been obtained with the contact measurement technique employed here for pressures approaching 60 psi. Copper gap-filling between nanofibers using electrochemical techniques is introduced as a means for providing mechanical stability as well as lateral heat spreading capabilities to the system. Further optimization of CNF growth, copper gap-filling, and measurement methodology will be needed to improve on the promising results obtained here as we work toward implementation of this novel material into IC packaging process flows.

References

(1) Kim, P.; Shi, L.; Majumdar, A.; McEuen, P. L. *Phys. Rev. Lett.* **2001**, *87*, 215502−1.
(2) Yang, D. J.; Zhang, Q.; Chen, G.; Yoon, S. F.; Ahn, J.; Wang, S. G.; Zhou, Q.; Wang, Q.; Li, J. Q. *Phys. Rev. B* **2002**, *66*, 165440.
(3) Wang, X.; Zhong, Z.; Xu, J. *Proc. 37th AIAA Thermophysics Conf.* **2004**, 2465.
(4) Yi, W.; Lu, L.; Dian-lin, Z.; Pan, Z. W.; Xie, S. S. *Phys. Rev. B* **1999**, *59*, 9015.
(5) Cruden, B. A.; Cassell, A. M.; Ye, Q.; Meyyappan, M. *J. Appl. Phys.* **2003**, *94*, 4070.
(6) Xu, J.; Fisher, T. S. *Proc. ITHERM* **2004**, 549.
(7) Chuang, H. F.; Cooper, S. M.; Meyyappan, M.; Cruden, B. A. *J. Nanosci. Nanotechnol.* **2004**, *4*, 964.
(8) Viswanath, R.; Wakharkar, V.; Watwe, A.; Lebonheur, V. *Intel Technol. J.* **2000**, Q3.
(9) *International Technology Roadmap for Semiconductors: Assembly and Packaging*, http://public.itrs.net.
(10) *The Electronics Industry Report 2004*; Prismark Partners LLC: New York, 2003.
(11) Kondo, K.; Yamakawa, N.; Tanaka, Z.; Hayashi, K. *J. Electroanal. Chem.* **2003**, *559*, 137.
(12) Ngo, Q.; Cruden, B. A.; Cassell, A. M.; Walker, M. D.; Ye, Q.; Koehne, J. E.; Meyyappan, M.; Li, J.; Yang, C. Y. *Proc. Mater. Res. Soc. Symp.* **2004**, *812*, F3.18.
(13) Vogt, M. R.; Polewska, W.; Magnussen, O. M.; Behm, R. J. *J. Electroanal. Chem.* **1997**, *144*, 113.
(14) Merkulov, V. I.; Melechko, A. V.; Guillorn, M. A.; Lowndes, D. H.; Simpson, M. L. *Appl. Phys. Lett.* **2001**, *79*, 2970.
(15) ASTM D 5470, "Standard Test Method for Thermal Transmission Properties of Thin Thermally Conductive Solid Electrical Insulation Materials", ASTM International.
(16) Koehne, J.; Li, J.; Cassell, A. M.; Chen, H.; Ye, Q.; Ng, H. T.; Han, J.; Meyyappan, M. *J. Mater. Chem.* **2004**, *14*, 676.
(17) Ren, Z. F.; Huang, Z. P.; Xu, J. W.; Wang, J. H.; Bush, P.; Siegal, M. P.; Provencio, P. N. *Science* **1998**, *282*, 1105.

NL048506T